Optics Letters

Full-color imaging with a 3D nanoprinted fiber endoscope

Longhui Huang,[1,2,†] Ziyi Huang,[1,2,†] Dejun Liu,[1,2,*] Chenyang Su,[1,2] Yalong Tai,[1,2] Min Wang,[3] Ying Wang,[1,2] Yiping Wang,[1,2] and Changrui Liao[1,2]

[1]Shenzhen Key Laboratory of Ultrafast Laser Micro/Nano Manufacturing, Guangdong and Hong Kong Joint Research Centre for Optical Fiber Sensors, State Key Laboratory of Radio Frequency Heterogeneous Integration, Shenzhen University, Shenzhen 518060, China
[2]Shenzhen Key Laboratory of Photonic Devices and Sensing Systems for Internet of Things, Key Laboratory of Optoelectronic Devices and Systems of Ministry of Education/Guangdong Province, College of Physics and Optoelectronic Engineering, Shenzhen University, Shenzhen 518060, China
[3]Photonics Center, State Key Laboratory of Radio Frequency Heterogeneous Integration, Shenzhen University, Shenzhen 518060, China
[†]These authors contributed equally to this work.
*anmeliu@163.com

Received 11 November 2025; revised 26 November 2025; accepted 1 December 2025; posted 1 December 2025; published 17 December 2025

Endoscopic technology plays a crucial role in minimally invasive diagnostic procedures and precision industrial inspections. However, producing a microsized full-color endoscope has been challenging in fabrication and aberration corrections. In this paper, we propose a miniaturized fiber endoscope featuring multiple lens elements with freeform surfaces using two-photon polymerization (TPP) 3D nanoprinting technology to effectively correct various optical aberrations and have realized good optical performances in full-color imaging. The microlens was integrated onto an imaging fiber tip, achieving a FOV of 60° and a resolution of 7.13 line pairs per mm (lp/mm). In addition, the proposed fiber endoscope is capable of accurately reproducing full-color information while preserving image details across different image types. This research offers an innovative approach to develop high-performance endoscopes and enhance its imaging applications.

https://doi.org/10.1364/OL.584435

Color information is essential in image and video processing as it closely aligns with human visual perception, providing realistic and vivid visual effects. In the medical field, color information helps accurately identify different tissues and pathological regions, enhancing the diagnostic accuracy of various devices. With the advancement of minimally invasive technology [1], higher demands have been placed on the size and performance of endoscopes. To accommodate the confined surgical spaces, endoscopes need to be miniaturized [1,2], while simultaneously improving imaging resolution, field of view, and enhancing color imaging capabilities to meet the increasingly stringent clinical demands. Endoscopes based on various working mechanisms have been proposed, such as lensless imaging schemes based on the measurement of the fiber transmission matrix (TM) [3,4]. However, due to fiber bending and twisting, these imaging methods are prone to significant distortion when reconstructing images and are often unable to effectively capture color information. Additionally, metalens is used as the objective lens of the endoscope, which can significantly reduce the size of the endoscope [5], but this method involves a strict tradeoff between working distance, depth of field, resolution, and FOV, with limited color imaging capabilities. Another solution involves the use of imaging fiber bundles, where each core within the bundle serves as an individual pixel. A straightforward imaging scheme adds a GRIN lens at the distal end [6], though this approach is limited by its resolution, a small and fixed working distance, and challenges in correcting optical aberrations.

Additive manufacturing technologies have become increasingly important in advanced manufacturing processes [7,8]. Among these, two-photon polymerization (TPP) 3D nanoprinting has demonstrated significant promise [9,10]. Unlike traditional photolithography, TPP technology allows for precise control of material solidification in three-dimensional space, offering extremely high spatial resolution of less than 100 nm. This capability has led to its widespread application in fields such as beam shaping [11–13], optical communications [14–16], and microfluidics [17–19]. Particularly in the domain of micro optics, TPP have demonstrated its unique potential for fabrication of complicated optical components with micron scale dimensions and superior optical performance across heterogeneous substrates [20–22]. The integration of TPP 3D printed microlens onto fiber endoscopes presents a promising strategy to enhance imaging quality, expand the FOV, and reduce the rigid tip length of endoscopic devices, thus significantly improving their clinical practicality [23].

In our previous work, a monochromatic imaging fiber endoscope was designed and experimentally demonstrated with the TPP 3D nanoprinting technology [24]. In this paper, we propose a full-color imaging fiber endoscope, a comprehensive workflow integrating optical design, fabrication, and characterization are presented. Both simulation and experimental analyses were conducted to evaluate the imaging performance of the

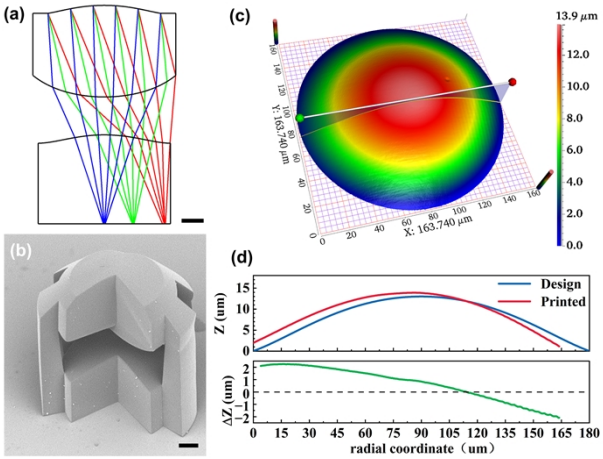

Fig. 1. (a) Geometric ray tracing results of the proposed objective dual lenses. (b) Scanning electron microscope image of the dual lens includes a 90° section cut. (c) Confocal microscope image of the topography of the microlens. (d) The upper graph displays the design height and printed height of the microlens, while the lower graph shows the deviation between the design height and the printed height. Scale bars, 30 μm.

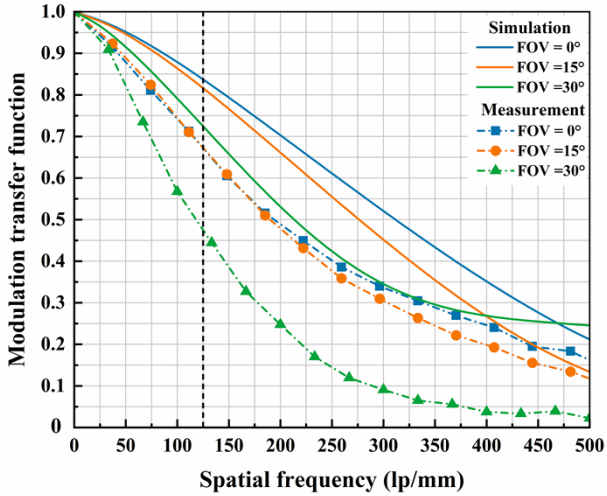

Fig. 2. Comparison of modulation transfer function simulation and experimental results at different FOVs.

endoscope, including resolution, FOV, modulation transfer function (MTF), and chromatic imaging capabilities. It is demonstrated that the proposed fiber endoscope was able to accurately render color images, highlighting its potential feasibility and future development prospects in practical applications.

The objective lens of the proposed fiber endoscope features a doublet microlens structure with a flat bottom surface in collection with the printing substrate (glass substrate and optical fiber endface in our experiment), as shown in Fig. 1(a). This configuration effectively mitigates edge warping during the manufacturing process while enhancing interfacial adhesion with substrates, thereby preventing delamination under mechanical perturbations. Geometric ray tracing methods were employed for microlens design. The microlens system was designed and optimized with a 60° FOV and a 180 μm entrance pupil diameter at the first lens surface, the total microlens dimensions were limited to less than 300 μm to avoid artifacts caused by stitching during the printing process. All other three surfaces of the doublet microlens were designed as aspherical and optimized accordingly, with the optimization process expressed by the equation in Eq. (1):

$$Z(r) = \frac{cr^2}{1+\sqrt{1-(1+k)c^2r^2}} + \sum_{i=1} A_{2i} r^{2i}. \quad (1)$$

IP-N162 (Nanoscribe GmbH) photoresist with a high refractive index (n = 1.62, V = 24.57) was selected to enable the reduction of lens curvature and minimizes incident angles at the interface [25], which collectively contribute to improved aberration correction. Furthermore, higher refractive index photoresist enables a reduction in the overall lens volume while maintaining excellent optical performance, thereby shortening processing times. For structural stability concerns, seven pillars were integrated into the lens design, ensuring precise alignment and mechanical robustness of the multi-lens system. The optimized simulation results show that the spot size increases with the field of view. At a half-field angle of 30°, the maximum RMS spot size is 2.31 μm, while the mirolens field curvature is controlled within 8 μm and the distortion is constrained to below 3%, as shown in Fig. S1 (Supplement 1).

All optical components were fabricated using a commercial two-photon polymerization 3D printer (Photonics Professional GT, Nanoscribe GmbH). We employed a 25× oil immersion microscope objective with a numerical aperture (NA) of 0.8 as the fabrication lens during the processing. The microlens fabrication parameters included a slice thickness of 0.1 μm, interlayer spacing of 0.1 μm, laser scanning speed of 50 mm/s, and processing power of 26 mW. Before the fabrication of the fiber endoscope, both ends of the imaging fiber were polished to achieve flat surfaces. After the micro lens was fabricated on the fiber end surface, it was immersed in PGMEA for 2 minutes and rinsed with IPA for 2 minutes.

A 90° sectional scanning electron microscopy image of the fabricated lens in Fig. 1(b) reveals a smooth surface with no noticeable defects. The top surface profile, measured via a confocal microscopy, is presented in Fig. 1(c), indicating a surface roughness of 30.8 nm. To assess the deviation between the printed and designed surface profiles, a cross-sectional line passing through the center of the lens was extracted and compared with the design values as shown in Fig. 1(d), the deviation between the designed and actual fabricated surface profiles is less than 2.5 μm. Minor shrinkage during the development process, along with the staircase effect caused by the layer by layer 3D nanoprinting process, led to deviations between the actual surface morphology and the designed contour. To test its imaging properties, microlens was first fabricated on glass substrates, and the detailed imaging results are provided in Supplement 1, Fig. S2. Experimental results of the resolution test chart show resolved imaging of element 6 of Group 2, corresponding to a resolution of 7.13 lp/mm. Imaging results of the Telefunken FuBK test chart, demonstrating effective chromatic aberration control across visible spectra, with no significant color fringing observed in test patterns.

MTF offers an effective means to assess an optical system's ability to reproduce object details. Figure 2 shows the MTF curves of the microlens simulated and measured at different fields of view. As the spatial frequency increases, the MTF values decrease, with a more pronounced performance degradation at larger field angles. Considering the relatively low pixel

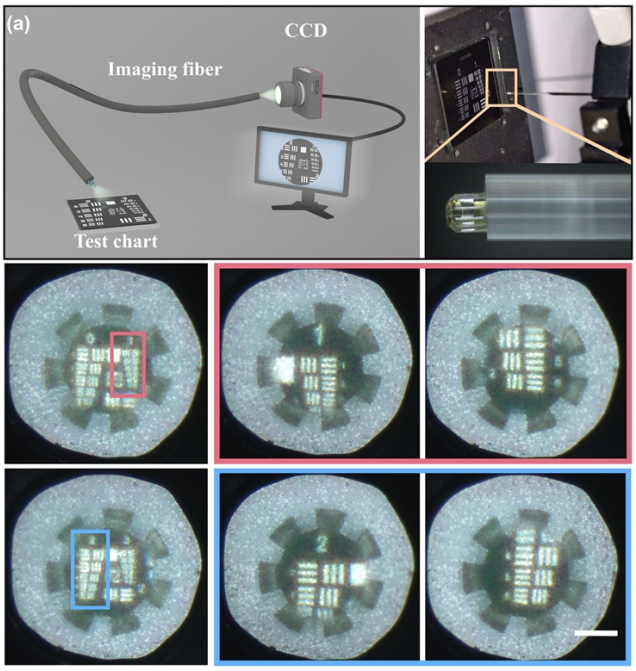

Fig. 3. Optical fiber endoscope and its resolution imaging testing. (a) A schematic diagram of the fiber endoscopy testing system and a photograph of the endoscope probe with the lower-right section displaying a magnified view of the probe. (b)–(d) Imaging of Groups 0 and 1 with the fiber endoscope. (e) and (f) Imaging of Groups 2 and 3 with the fiber endoscope. (Scale: 100 μm.)

density of imaging fibers compared to CMOS sensors, the Nyquist sampling theorem indicates that sufficient MTF performance at 125 line pairs per mm (lp/mm) is adequate for endoscopic applications. In a photographic system, the Modulation Transfer Function value must exceed 0.1 to be resolvable by the image sensor. The measured MTF exceeds 0.45 at 125 lp/mm, fully satisfying the operational requirements for imaging fibers, ensuring sufficient clarity and resolution even in the peripheral field of view.

A miniaturized fiber endoscope and its imaging properties are characterized in Fig. 3. A schematic diagram of the fiber endoscope testing system and a photograph of the fiber endoscope are shown in Fig. 3(a). The imaging fiber, purchased from the Xi'an institute of optics and precision mechanics, has a diameter of 460 μm and a numerical aperture (NA) of 0.35, it contains approximately 12,000 cores with each core having a diameter of 4 μm and a core spacing of 1 μm. The imaging quality across different regions of the USAF 1951 target was evaluated using the testing system depicted in Fig. 3(a) in conjunction with the fiber endoscope. Figure 3(b) presents the full-field image of Group 0–1. This image covers an information-rich area, where the spacing of the stripes is resolvable, though slightly blurred. In contrast, Figs. 3(c) and 3(d) present localized views of element 1 of Group 1, where the details are clearer. In Group 1, the boundaries of the black-and-white stripes and numerical markings are clearly distinguishable. Figure 3(e) shows the full-field image of Groups 2-3. Although these groups contain smaller features compared to Group 0-1, the imaging performance demonstrates similar quality. Figures 3(f) and 3(g) show the magnified views of element 6 of Group 2. It can be observed that the lines in Group 2 remain clearly distinguishable. We also

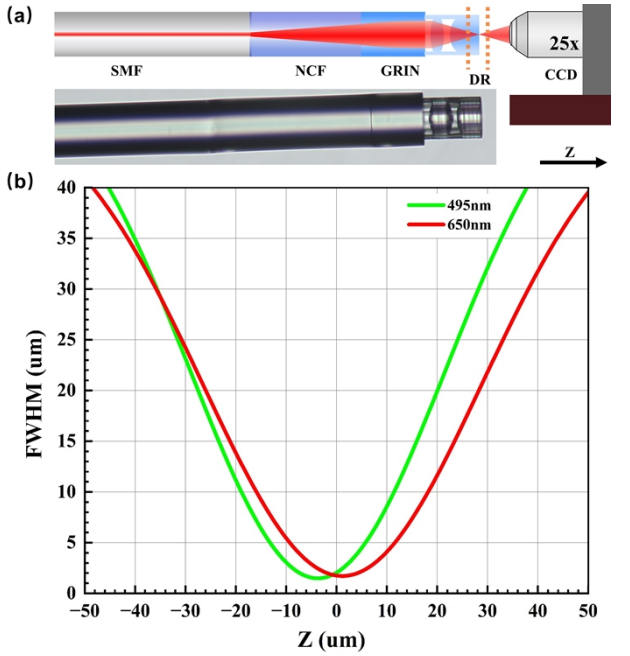

Fig. 4. (a) Schematic diagram of the chromatic aberration testing system, with the fabricated test probe shown below. (b) Measured FWHM distribution for 495 and 650 nm at different Z-Positions, with Z steps of 0.5 μm.

examined the elements of Group 3, but were unable to distinguish its line pairs. Therefore, the proposed fiber endoscope is capable of resolving element 6 of Group 2, corresponding to a resolution of 7.13 lp/mm, and its imaging quality is superior to previous results [23,24].

To quantify the chromatic aberration of the proposed microlens, a beam analyzer was used to measure the full width at half maximum (FWHM) of the light spot at different Z-positions near the focal point for different wavelengths of 495 and 650 nm. The focal position was determined by measuring the minimum beam FWHM. To achieve this, a section of no-core fiber was spliced to a single-mode fiber to expand the beam, and then a section of GRIN fiber (1/4 pitch length) was spliced after the no-core fiber to produce a collimated beam. The proposed microlens was then inverted and fabricated on the end face of the GRIN fiber, as shown in the structural and physical diagrams in Fig. 4(a). The FWHM was measured in a 100 μm range in the Z-direction before and after the focal plane using a high-precision translation stage, with the results shown in Fig. 4(b). The beam FWHM for both wavelengths shows the minimal values at the focal point and gradually expands when moving away from the focus. The focal point at 495 nm occurs earlier than at 650 nm, which is attributed to the higher refractive index of materials with normal dispersion at shorter wavelengths, leading to faster beam convergence. The focal shift between the two wavelengths is approximately 5.0 μm, indicating a slight focal offset due to chromatic aberration. It is worth noting that this 5.0 μm difference is comparable with the previous reported microlens [26]. To further mitigate chromatic aberration, materials with varying Abbe numbers or hybrid refractive-diffractive designs can be employed to achieve achromatic performance [25].

We evaluated the full-color imaging capabilities of the fiber endoscope by testing its performance on a variety of chromatic

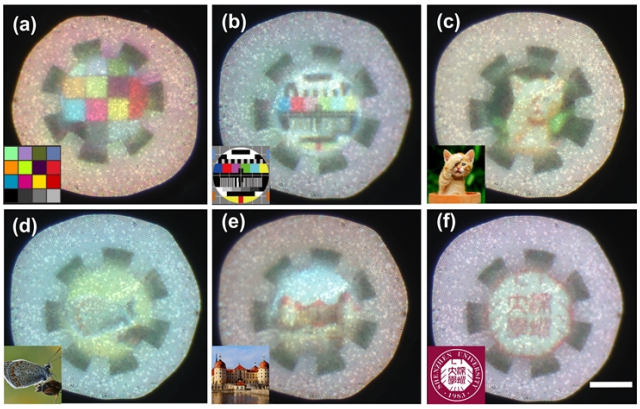

Fig. 5. Presents chromatic imaging results of the fiber endoscope. (a) Multicolor grid chart. (b) Telefunken FuBK test card. (c) Orange tabby cat. (d) Gray butterfly. (e) Architectural structure of a castle. (f) Shenzhen University emblem. The inset in the lower-right corner of each figure shows the picture used for the imaging test. (Scale: 100 μm.)

targets. Figure 5(a) shows the imaging results of a color chart, demonstrating clear differentiation of color distributions and authentic color reproduction. Figure 5(b) illustrates the performance on the Telefunken FuBK test chart, featuring standardized color patches with smaller dimensions and increased detail complexity. Figure 5(c) presents a lateral view of an orange tabby cat, where the system faithfully reproduces natural fur coloration, eye pigmentation, and skin tones with high chromatic fidelity. Figure 5(d) depicts a gray butterfly, capturing fine details of brown spots against the gray wings. Figure 5(e) showcases architectural imaging of a castle, with the endoscope accurately rendering façade elements, including wall surfaces and window details, while effectively conveying three-dimensional layering of the structure. Figure 5(f) displays the imaging results of the text information in the center of the Shenzhen University emblem. The system effectively preserves accurate color reproduction and fine detail resolution across different image types. While current endoscopic imaging exhibits pixelation artifacts, this limitation can be mitigated through the application of advanced image processing techniques [27].

In summary, we successfully designed and fabricated a full-color fiber endoscopic microlens using TPP 3D nanoprinting technology. The microlens was integrated on an imaging fiber, enabling comprehensive endoscopic evaluation through resolution target imaging at various positions and chromatic imaging tests involving color blocks, biological specimens, architectural structures, and textual information. The experimental results indicate that the microlens achieves a FOV of 60° and a resolution of 7.13 line pairs per mm (lp/mm), and the fiber endoscope system exhibited superior chromatic performance across diverse imaging targets, effectively maintaining color fidelity and detail reproduction. These findings highlight the significant advantages of TPP 3D nanoprinting microlens for endoscopic applications, including high precision, enhanced resolution, miniaturization potential, and design customization.

Funding. National Key Research and Development Program of China (2024YFB3213700); National Natural Science Foundation of China (62475170, 62475161, U22A2088); Basic and Applied Basic Research Foundation of Guangdong Province (2022B1515120061, 2023A1515012893); Shenzhen Science and Technology Innovation Program (ZDSYS20220606100405013, JCYJ20220818095800001, JCYJ20220818095615034); Research Team Cultivation Program of Shenzhen University (2023QNT009); Medicine Plus Program of Shenzhen University (2024YG013); Scientific Foundation for Youth Scholars of Shenzhen University (806-0000340601).

Disclosures. The authors declare no conflicts of interest.

Data availability. Data underlying the results presented in this paper are not publicly available at this time but may be obtained from the authors upon reasonable request.

Supplemental document. See Supplement 1 for supporting content.

REFERENCES

1. B. Wang, Q. Zhang, X. Chen, *et al.*, J Microsc. **288**, 87 (2022).
2. H. Wang, N. Zhang, and S. Zuo, Appl Opt. **57**, 1554 (2018).
3. N. Shekel and O. Katz, Opt. Lett. **45**, 4288 (2020).
4. U. Weiss and O. Katz, Opt. Express **26**, 28808 (2018).
5. J. E. Fröch, L. Huang, Q. A. A. Tanguy, *et al.*, eLight **3**, 13 (2023).
6. G. Oh, E. Chung, and S. H. Yun, Opt. Fiber Technol. **19**, 760 (2013).
7. H. Zhu, C. Yao, B. Wei, *et al.*, Int. J. Extreme Manuf. **5**, 042004 (2023).
8. S. Hu, X. Huan, Y. Liu, *et al.*, Int. J. Extreme Manuf. **5**, 032009 (2023).
9. H. Wang, W. Zhang, D. Ladika, *et al.*, Adv. Funct. Mater. **33**, 2214211 (2023).
10. S. O'Halloran, A. Pandit, A. Heise, *et al.*, Adv. Sci. **10**, 2204072 (2023).
11. Z. Li, B. Li, D. Liu, *et al.*, Opt. Laser Technol. **167**, 109798 (2023).
12. C. Su, Z. Li, D. Liu, *et al.*, J. Lightwave Technol. **43**, 3968 (2025).
13. T. Gissibl, M. Schmid, and H. Giessen, Optica **3**, 448 (2016).
14. C. R. Ocier, C. A. Richards, D. A. Bacon-Brown, *et al.*, Light Sci Appl. **9**, 196 (2020).
15. A. J. Littlefield, J. Huang, M. L. Holley, *et al.*, Optica **11**, 995 (2024).
16. Z. L. Wu, Y. N. Qi, X. J. Yin, *et al.*, Polymers (Basel) **11**, 553 (2019).
17. S. Soheili, E. Mandegar, F. Moradikhah, *et al.*, J. Drug Deliv. Sci. Technol **61**, 102268 (2021).
18. Z. Faraji Rad, R. E. Nordon, C. J. Anthony, *et al.*, Microsyst. Nanoeng **3**, 17034 (2017).
19. F. Mayer, S. Richter, J. Westhauser, *et al.*, Sci. Adv. **5**, eaau9160 (2019).
20. K. Weber, Z. Wang, S. Thiele, *et al.*, Opt Lett. **45**, 2784 (2020).
21. M. Schmid, S. Thiele, A. Herkommer, *et al.*, Opt Lett **43**, 5837 (2018).
22. S. Thiele, K. Arzenbacher, T. Gissibl, *et al.*, Sci. Adv. **3**, e1602655 (2017).
23. T. Gissibl, S. Thiele, A. Herkommer, *et al.*, Nat. Photonics **10**, 554 (2016).
24. B. Li, C. Liao, Z. Cai, *et al.*, Fundam. Res. **4**, 123 (2024).
25. M. Schmid, F. Sterl, S. Thiele, *et al.*, Opt Lett. **46**, 2485 (2021).
26. S. Ristok, S. Thiele, A. Toulouse, *et al.*, Opt. Mater. Express **10**, 2370 (2020).
27. J. Wu, T. Wang, O. Uckermann, *et al.*, Sci. Rep. **12**, 18846 (2022).